

Article

The Optimum Process to Produce High-Strength Cast/Forged Al–8%Zn–2.5%Mg–1%Cu Alloy

Teng-Shih Shih ^{1,*}, Ei-Ting Kwang ¹ and Yung-Sen Huang ²

¹ Department of Mechanical Engineering, National Central University Jhong-Li district, Taoyuan 32001, Taiwan

² Lio-Ho Machine Work Company, Taoyuan 32056, Taiwan

* Correspondence: t330001.ncu@gmail.com; Tel.: +886-3-425-4501

Received: 26 July 2019; Accepted: 29 August 2019; Published: 3 September 2019



Abstract: Al–8Zn–2.5Mg–1Cu alloy casting blocks were subjected to homogenization and annealing. The treated blocks were then held at different temperatures and forged in different dies to obtain 20 mm-thick plates. After T73 heat treatment, the plates were cut and machined to obtain tensile bar samples that were further subjected to tensile and potentiodynamic polarization tests. Upon analyzing the experimental results, the subzero-treated and forged samples (SO) developed fine grains in their matrix and displayed yield stress (YS) about 400 MPa and an elongation of 11%. The hot-forged samples (HC) displayed a relatively higher YS slightly >440 MPa and a lower elongation of 4%. The intermetallic compound particles confined to the HC decreased its corrosion resistance to be worse than that of the SO. All anodized and sealed samples effectively improved their corrosion resistance. Due to its fine grains, the anodized SO sample produced a higher I_{corr} than the anodized HC sample.

Keywords: hot forge; subzero-treated; dynamic recrystallization; corrosion resistance

1. Introduction

Al– x Zn– y Mg– z Cu alloys (where $x = 5$ –8%; $y = 2$ –4%, Cu = 0–2%) are high-strength precipitation-hardening aluminum alloys. These alloys can develop a YS >400 MPa with an adequate elongation (>10%). The main drawback in using these alloys is the issue of stress-dependent corrosion [1–5]. Hence, these alloys are commonly used after overage treatment.

The precipitates of Al– x Zn– y Mg– z Cu alloys include stable η (MgZn₂), T(Al₂Mg₃Zn₃), S(Al₂CuMg), and θ (Al₂Cu). The sequence of precipitation for these alloys is generally summarized as SSS → GP zones → η' → η . Phases of η' and η can be observed in the grain boundary and the matrix after T6 heat treatment. With increasing aging time and temperature, η phases can be observed dominantly in the grain boundary and the matrix, accompanied by some η' phases [6–10].

Forging Al alloys could offer good tensile strength (≥ 300 MPa) and high elongation ($\geq 10\%$) and fatigue strength (≥ 120 MPa at 1×10^7 cycles) [11–13]. The forged parts are widely used in the automotive industry. The conventional forging process uses forging blocks that are sliced from extruded bars or plates. Preform and/or two-stage hot forging process are regularly adopted to obtain near-net-shape parts. After trimming the flashes, the forged parts are removed for heat treatment to account for the strength obtained from precipitation hardening. The 6xxx series alloys and 7xxx alloys are commonly subjected to T4/T6 and T4/T73 heat treatment, respectively. The restrike process is a step necessary to correct the parts distorted upon heat treatment. Therefore, the whole process takes a relatively long processing time and creates a cost issue compared with other forming processes. High-pressure die casting is characterized by a high production rate of near-net-shape casting, but the casting parts often lack appropriate elongation (commonly lower than 5%). This process is not recommended for making

knuckles in the automobile sector. The tilted gravity casting process is now currently used to produce parts fitting for job-shop factories. Its production rate is low, which makes it difficult to satisfy the market demand of automobile industry.

The concept of the cast/forge process was proposed by Fujikawa et al. [14] Chang et al. introduced the cast/forge hybrid process to reduce the porosity of 7075 aluminum alloy castings [15]. The tripods produced with this process were shown at ALUMINUM CHINA 2018, Shanghai, New International Expo Centre (2018/07/11–13). The block castings were used instead of extruded bars or plates to decrease the processing cost. Hot forging often generates a dense deformation texture in the substrate but would induce distortion during heat treatment, as mentioned previously. Instability tended to appear at high strain rates ($0.18\text{--}1\text{ s}^{-1}$), when the Al–5Zn–2.5Mg–1.5Cu alloy was heated over the temperature range of 593–753 K. The optimum hot working parameters were found to be at 753 K, with a strain rate of $0.01\text{--}0.1\text{ s}^{-1}$ for coarse grains and fine grains [16]. Working with a low strain rate significantly increased the production cost when the Al–Zn–Mg–Cu alloy was processed to make automobile parts. The cast/forge hybrid process could become an alternative for forming Al–Zn–Mg–Cu alloys, if a high strain rate could be successfully adopted in the process to make appropriate automobile parts.

Forging at a low temperature decreases the formability of metal parts. Nevertheless, the deformation temperature and strains affect the dynamic recrystallization (DRX) or dynamic recovery (DRV) in Al alloys. As a result, the optimum mechanical properties could be generated by forming or forging at a low temperature. This study proposes a hybrid process of forging Al alloys at a low temperature to acquire 60–70% completion in the final shape by utilizing an open-die set. After heat treatment, the parts will undergo machining to get machined parts. This hybrid process (cast block forged at a low temperature followed by machining) is expected to produce optimum microstructure control thereby reducing or eliminating the distortion caused by heat treatment. This concept was applied in this study to treat the blocks at a sub-zero temperature and then forge by open die (these are indicated as subzero-treated (SO) samples in the study).

2. Materials and Methods

Commercial Al–5%Zn–2.5%Mg–1.5%Cu billets were used as the base metal and were melted in a 30 kg induction furnace. To produce the desired alloy samples, small amounts of Al–10% Zr master alloys and pure Zn (99.9%) were added to the molten metal. The pouring temperature was set at 1000 K, and the metal mold temperature was held at 373–423 K [13]. After solidification, the top risers of the Y-block castings were removed to obtain 40 mm × 50 mm × 100 mm block castings. Their chemical compositions are listed in Table 1.

In this study, a Y-block mold with a top riser, which enhanced the feeding behavior of the solidified metal. In our previous study, we checked the soundness of a poured Y-block by using A356 and 6061 alloys. Castings were prepared by using a proper pouring temperature and the abovementioned metal mold temperature. The block castings were sound without visible porosities or shrinkages. Additionally, the defects entrapped in the block castings, such as dross or oxide particles with size larger than 30 μm , were found to display a degraded elongation lower than 10% after forging/heat treatment.

Table 1. Chemical compositions of as-cast samples (wt %).

| Element | Si | Fe | Cu | Mn | Mg | Cr | Zn | Ti | Zr |
|---------|------|------|------|------|------|------|------|------|------|
| Content | 0.07 | 0.15 | 1.65 | 0.04 | 2.42 | 0.21 | 8.39 | 0.02 | 0.18 |

The block castings underwent a three-step homogenization: holding at 723 K for 12 h, at 623 K for 24 h, and at 753 K for 12 h [17], and then annealing heat treatment at 686 K for 2 h. The casting blocks were divided into two groups. One group was frozen to 195 K, held in dry ice for 600 s, and then forged using a set of open dies to reduce the thickness by 50%. This set of samples were coded as SO. The other group was heated to 593 K and forged using a set of closed dies to reduce

the thickness by 50%. These samples were coded as hot-forged (HC). A 600 ton hydraulic press was employed in the forging process with a compression speed of about 2–3 mm/s. The strain rate of deformation was in the range of $1\text{--}10^1\text{ s}^{-1}$. The dimensions of the closed die are shown in Figure 1a–c. After forging, the blocks were removed, solution-treated at 748 K for 90 min, and then quenched in chilled water at 277 K. Subsequently, the blocks underwent T73 artificial aging treatments at 383 K for 8 h and at 448 K for 8 h. All heat-treated blocks that were coded as HZrT73 (HC) and HZrT73 (SO) were machined to produce tensile test bars with a gage diameter of 9 mm. The tensile properties were determined on the basis of an average of four tests. No visible defects, such as pores or dross, were detected in the fractured tensile bars when the data were analyzed. After the tensile tests, the tested bars were sliced to produce disk-shaped samples for microstructure observation using optical micrographs, field emission scanning electron microscopy (SEM) coupling with energy-dispersive X-ray spectroscopy (EDS, FEI Nova NanoSEM 230, Thermo Fisher Scientific, Hillsboro, OR, USA), electron backscatter diffraction (EBSD NordlysMax3, Tokyo, Japan), and transmission electron microscopy (TEM). The setting conditions for the EBSD test were as follows: the accelerating voltage was 20 kV, and the specimen was tilted 70° . Samples for the TEM test were prepared from FIB (focused ion beam, Hitachi NX2000, Hitachi High-Technologies Corporation, Tokyo, Japan). TEM was conducted with an operating voltage of 200 kV by JEOL (JEM-ARM200FTH, Tokyo, Japan).

The specimens for microscopic observation were prepared from the roots of tensile bars; these bars were sliced from the strained forged plates. Samples were anodized using a 15% H_2SO_4 solution at room temperature for 40 min with a current density of 2.153 A/cm^2 to obtain a $20\text{ }\mu\text{m}$ anodic oxide film [18]. The anodized samples were sealed in a hot water bath (373 K) for 80 min.

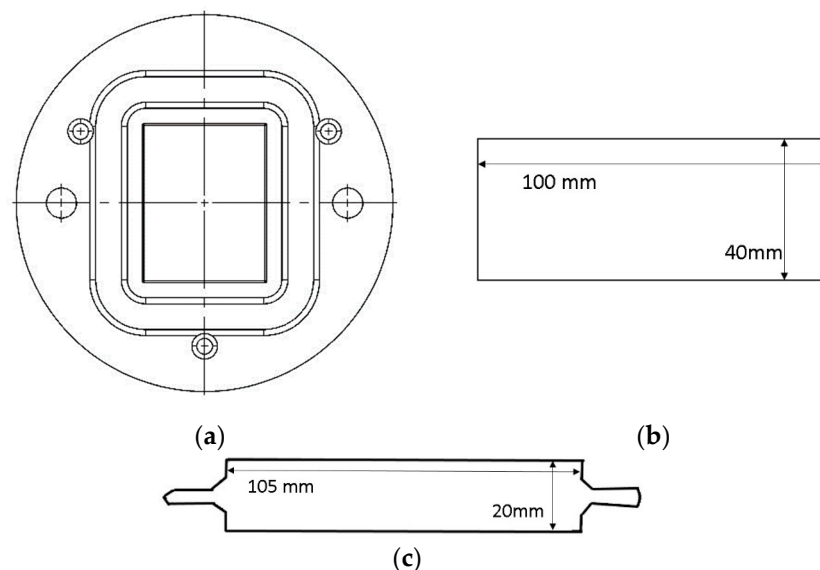


Figure 1. (a) Drawing of the closed die, (b) block sample before forging (50 mm × 100 mm × 40 mm), and (c) forged plate (82 mm × 105 mm × 20 mm).

Potentiodynamic polarization tests were conducted on different heat-treated samples, and the results were recorded using an Autolab PGSTAT30 Potentiostat [19]. The polarized potential of the tested sample was returned to its rest potential, and the anodic polarization curve was obtained by increasing the potential (with a scan rate 0.01 V/s) toward the noble direction until a voltage of 2 V was reached for the sealed film. All polarization curves were obtained from an average of five measurements.

3. Results and Discussion

The mechanical properties of the HC and SO samples were tested (listed in Table 2; standard deviations are also included in parentheses). When pouring Al alloys, it is difficult to exclude microscopic defect such as micron-scale oxide particles. In the experiment, we found that when the oxide particle size was less than 30 μm , no significant degradation of the elongation occurred.

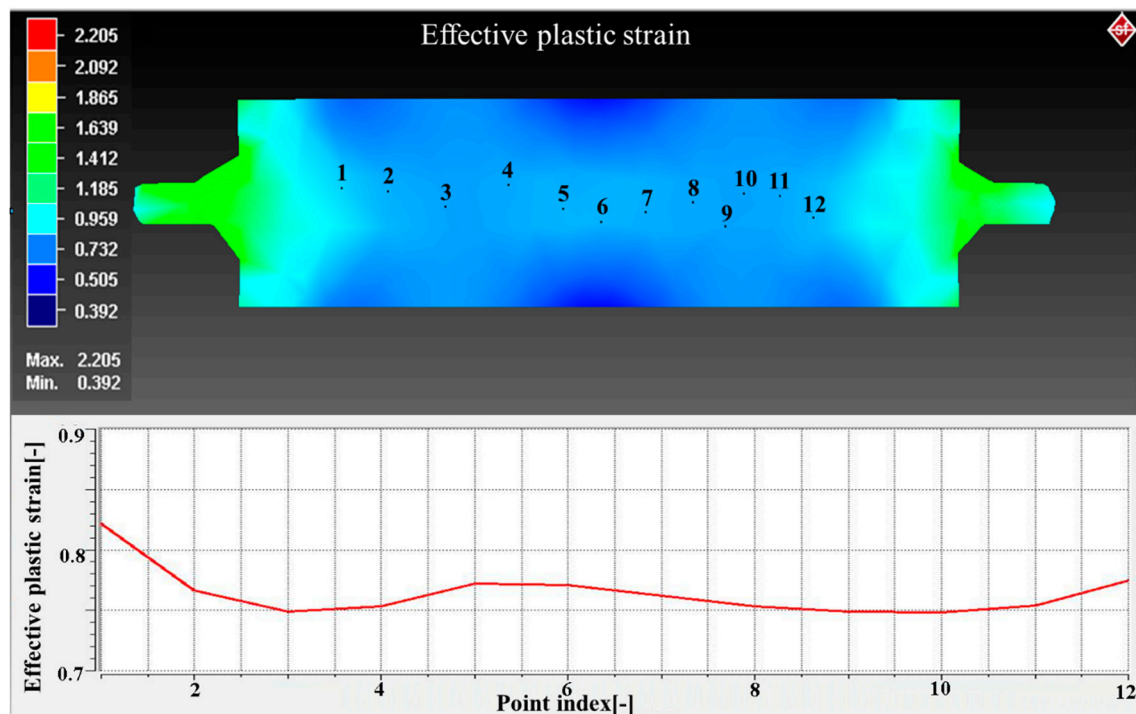
Samples that were hot-forged (HC) using a closed die exhibited stronger strengths of ultimate tensile stress (UTS 508.2 MPa) and YS (440.2 MPa) than subzero-treated (SO) samples. The SO samples displayed moderate strengths of UTS (484 MPa) and YS (407 MPa), with a superior elongation (11.8%) compared with the HC samples (4.2%). A small deviation in the measured strengths of the SO samples was observed. Factors that caused such differences may include the working temperatures that altered the microstructure in the samples' matrix.

Table 2. Measured tensile properties for hot-forged (HC) and subzero-treated (SO) samples.

| Sample Code | UTS (MPa) | YS (MPa) | TEL. (%) |
|-------------|------------|------------|----------|
| HC: Avg./SD | 508.2/33.4 | 440.2/46.8 | 4.2/1.3 |
| SO: Avg./SD | 484/1.4 | 406.8/4.7 | 11.8/2.4 |

Avg: average; SD: standard deviation; UTS: ultimate tensile stress; YS: yield stress; TEL: total elongation.

The sample blocks underwent compression in both the open and the closed die during forging. Two groups of deformed blocks experienced a reduction of 50% in thickness. Figure 2a,b display, respectively, the effective strains acting on HC and SO samples during forging. Table 3 lists the parameters used for simulation, where n is the strain hardening exponent, and K is the strength coefficient (MPa). The locations for preparing tensile specimens were at regions between points 2 and 5 and points 7 and 10. Each forged plate was used to produce two pieces of tensile bars. The effective strains for two groups of samples were close. Generally, there were merely minor differences in the deformed strains for HC and SO samples.



(a)

Figure 2. Cont.

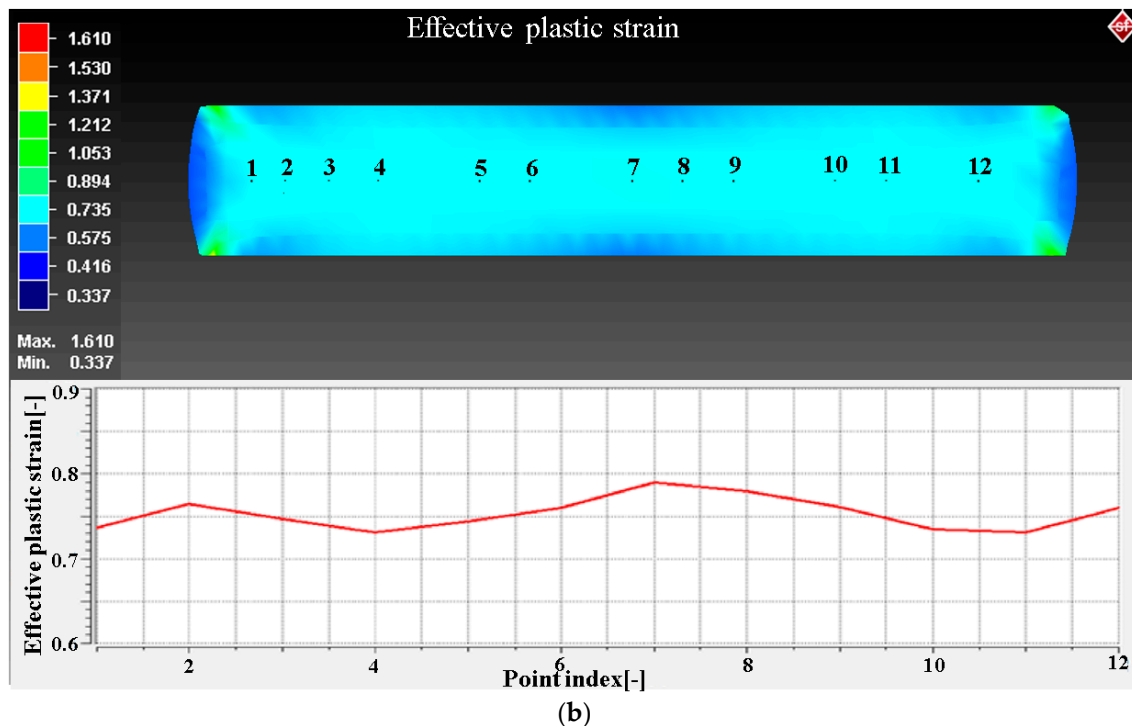


Figure 2. Simulation results of the effective strains produced from the deformed samples by using a set of (a) closed dies (hot forge); and (b) open dies (cold forge).

Table 3. Parameters used for simulation in Simufact software analyses.

| Poisson Ratio | n | K (MPa) | CTE (CD) (1/K) | CTE (OD)(1/K) | C_p (J/kg—K) | q (W/m—K) |
|---------------|------|---------|-----------------------|-----------------------|----------------|-------------|
| 0.33 | 0.17 | 400 | 2.52×10^{-6} | 2.16×10^{-6} | 960 | 173 |

CTE: coefficient of thermal expansion; C_p : specific heat capacity; q : thermal conductivity. CD: close die; OD: open die.

The materials used in this study contained Mg-2.5 wt% and Zn-8 wt% alloys. Mg and Zn alloys in aluminum can significantly decrease its stacking fault energy [20]. As a result, DRX occurred preferentially in the deformed samples. Figure 3a–c display the matrix morphologies of the SO sample after forging, partial solution (475 °C/45 min), and full solution (475 °C/90 min), respectively. The white spots in Figure 3a represent fine grains in the deformed matrix after forging. These fine grains formed because polygonization occurred, reorganizing grain dislocations. Assisted by the heat of the solution treatment, the grains gradually increased their size, as shown in Figure 3b,c.

Jonas and colleagues claimed that DRX is initiated at the critical strain and critical stress leading to softening of the deformed substrate in metals. Further increasing stress or deformation increases the dislocations in the work-hardening grains [21]. The forming temperature increases to favor DRX for a given strain rate [22]. The SO sample deformed at 195 K to partly suppress DRV and to accumulate grain dislocations. After heat treatment, the tangling dislocations formed fine grains by polygonization, producing high-angle grain boundaries, as shown in Figure 4b. In contrast, the HC sample was hot-deformed, and DRX prevailed during deformation. As a result, the deformed and heat-treated substrate showed coarse grains with mostly low-angle grain boundaries, as shown in Figure 4a.

Di Feng et al. studied the hot deformation behavior of Al-7.7Zn-2.1Mg-2.0Cu-0.12Zr alloy at temperatures of 573–823 K and true strain rates of 0.01–10 s⁻¹. They discovered that DRX occurred at processing conditions of temperature in the range of 680–823 K and strain rate of 0.05–1 s⁻¹ [23]. The above processing conditions are close to those used for the HC samples in the current experiment. DRX in the HC samples was further confirmed.

The matrix of HC samples exhibited coarse grains with a low level of grain boundary area. Consequently, the HC sample's matrix contained more fine precipitates within grains compared to the

SO sample's matrix. These fine precipitates were mostly stable η (MgZn_2) and meta-stable η' (MgZn_2) phases, as shown by TEM photographs in Figure 5a,b, respectively, for SO and HC samples. These precipitates strengthened the matrix of HC samples leading to high UTS and YS.

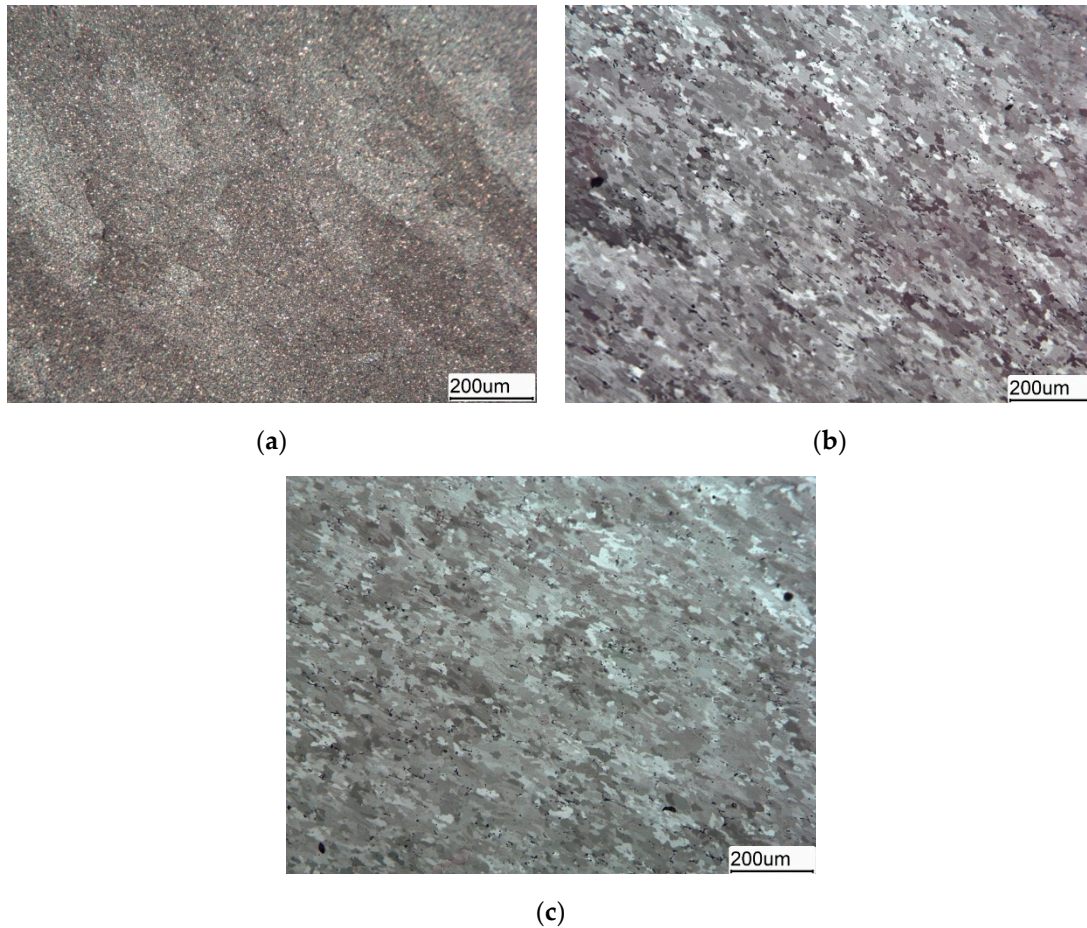


Figure 3. Optical micrographs for an SO sample; (a) after forging at low temperature, (b) after solution at 475 °C for 45 min, and (c) after solution at 475 °C for 90 min.

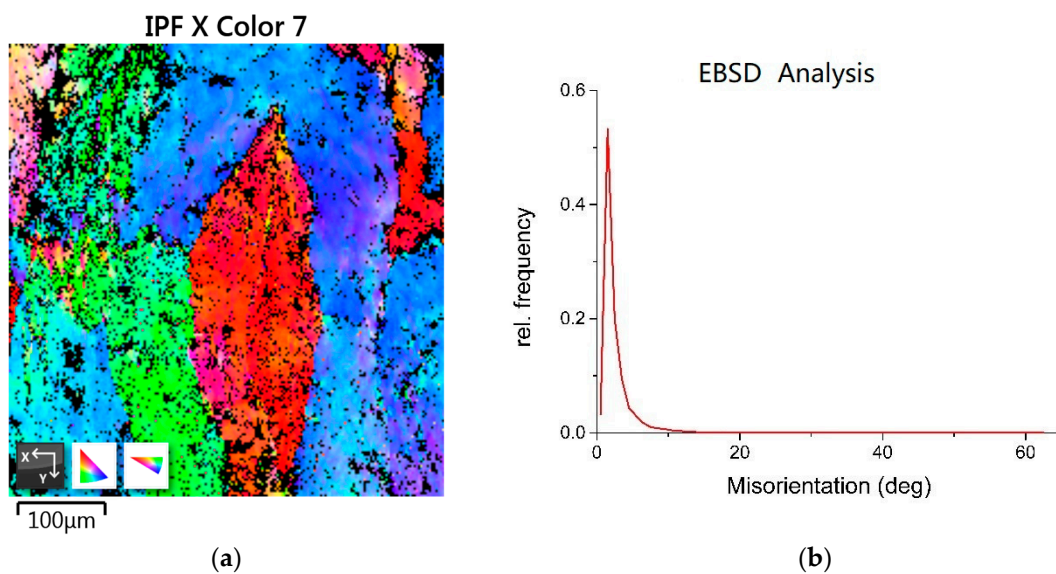


Figure 4. Cont.

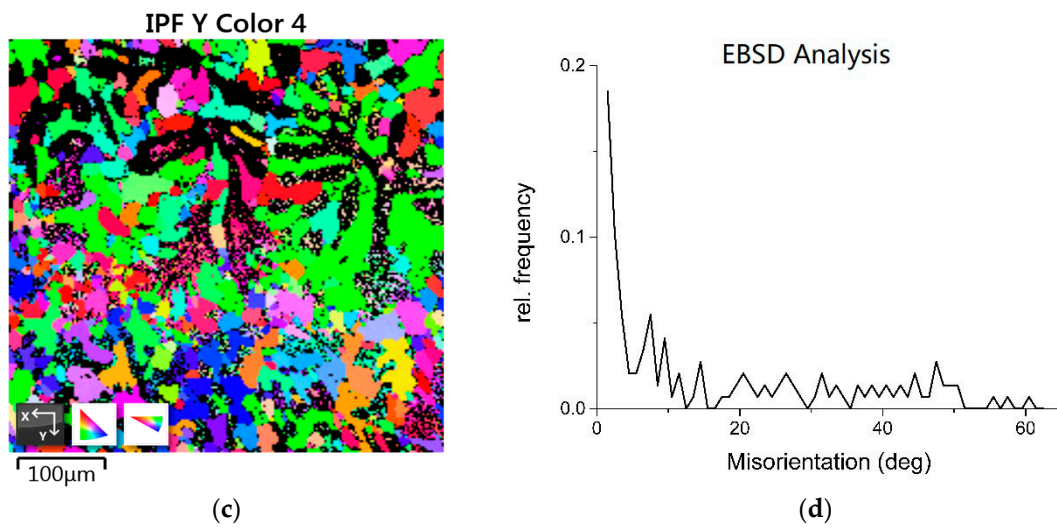


Figure 4. EBSD analyses of the grains with different misorientation grain boundary angles; (a,b) for HC sample; (c,d) for SO sample.

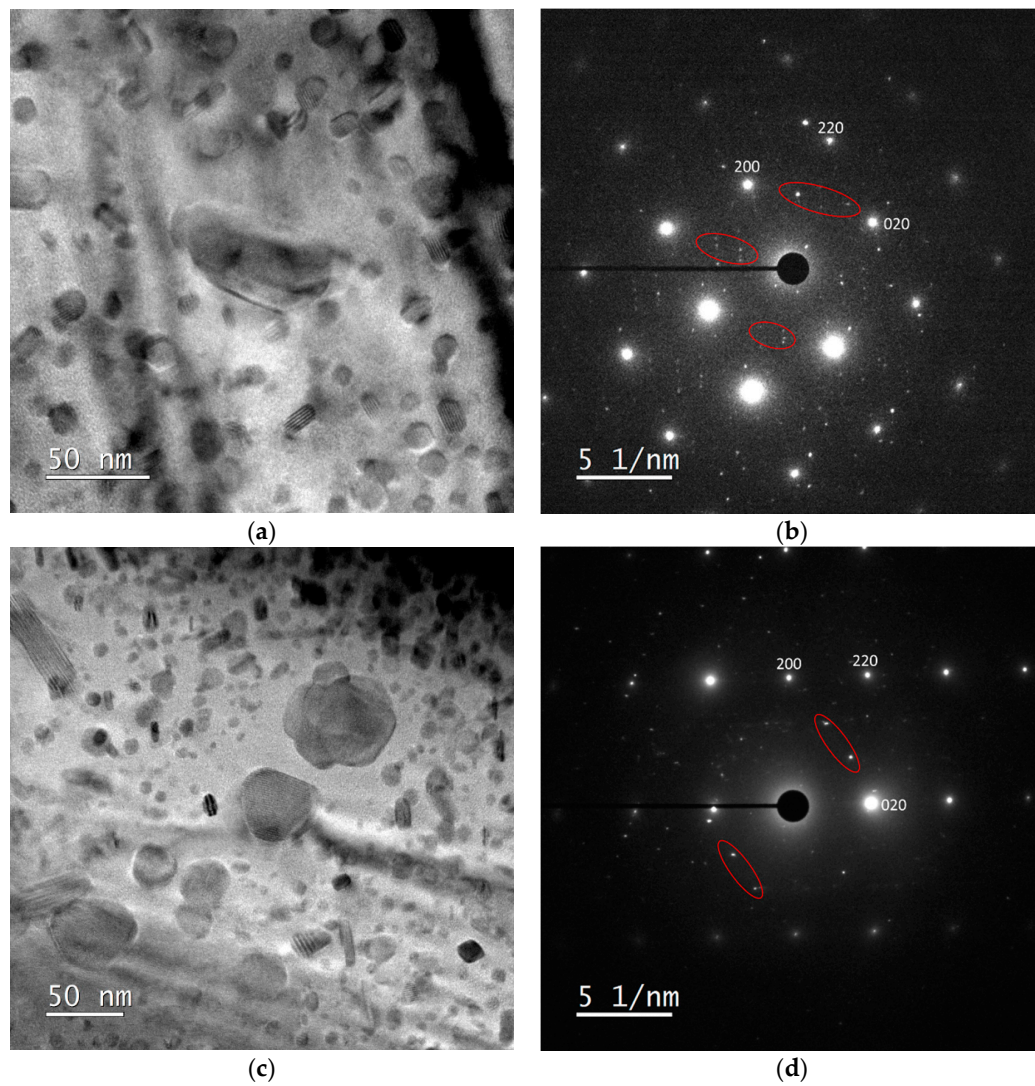
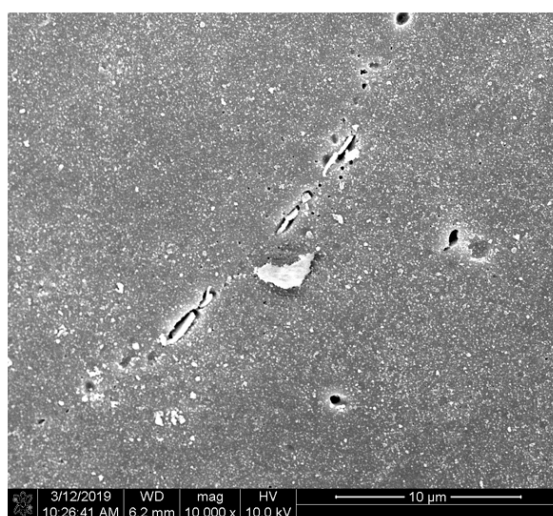


Figure 5. TEM photographs and diffraction patterns of MgZn₂ precipitate in (a,b) SO sample; (c,d) HC sample.

Grain boundaries locate (or store) dislocations. Precipitates are readily incubated, nucleate, and grow at grain boundaries. Abolhasani et al. and Fan et al. discovered that Cu atoms in the solution of an Al–Mg–Zn–Cu alloy promoted nucleation of Al₂CuMg [1,24]. Some precipitates that located and lined up at the grain boundaries in the HC sample contained Cu, Mg, and Zn atoms, as observed in Figure 6. The precipitates readily grew in size through high diffusivity at grain boundary to form particles. The precipitates situated within grains were likely to be Al₂CuMg, as can be observed in the TEM images (Figure 7a,b for SO and HC samples, respectively). These fine precipitates mainly strengthened the matrix of the samples. The HC sample exhibited coarse grains in combination with lined-up Al–Cu–Mg–Zn particles at grain boundaries, thereby resulting in a lower elongation with respect to the SO sample.



| Element | Atom(at.%) |
|---------|------------|
| Al | 84.72 |
| Mg | 5.02 |
| Zn | 6.19 |
| Cu | 4.07 |

Figure 6. Al–Cu–Mg precipitates located and lined up at the grain boundaries in the matrix of the HC sample.

Polarization curves were determined for the HC and SO samples, as shown in Figure 8a,b, respectively. The SO samples (−1.13 V) showed higher corrosion resistance than the HC samples (−1.30 V), and the pitting potential E_{pit} (SO: −0.79 V and HC: −0.75 V) was similar in each sample (Table 4). The differences in microstructure, such as precipitates and grain size, as discussed previously, have effects on E_{corr} . The SO samples displayed small standard deviations in the tested E_{corr} and I_{corr} . The intermetallic compound (IMC) retained in the matrix of different samples should be responsible for such differences. The HC samples contained more IMC particles than the SO samples (Figure 9a,b). EDS analyses demonstrated that these IMC particles contained Cu, Mg, and Zn alloys. These IMC particles accelerated the corrosion behavior when the samples were in contact with an electrolyte.

Anodization and sealing can improve the corrosion resistance of SO and HC samples and especially improve their pitting resistance. This study revealed that almost no pitting occurred during the corrosion test on the anodized and sealed samples. The anodized/sealed SO sample demonstrated a relatively lower I_{corr} than the anodized/sealed HC sample (an SO sample of 3.29×10^{-6} A/cm² compared with an HC sample of 7.97×10^{-6} A/cm²). This material also displayed corrosion resistance comparable with that of anodized/sealed extruded AA7075-T73 bar samples; E_{corr} : −0.91 V for the SO sample and −0.61 for the extruded bar sample, I_{corr} : 3.29×10^{-6} A/cm² for the SO sample and 3.9×10^{-6} A/cm² for the extruded bar [11]. No pitting was observed in both anodized/sealed SO and extruded AA7075 bar samples.

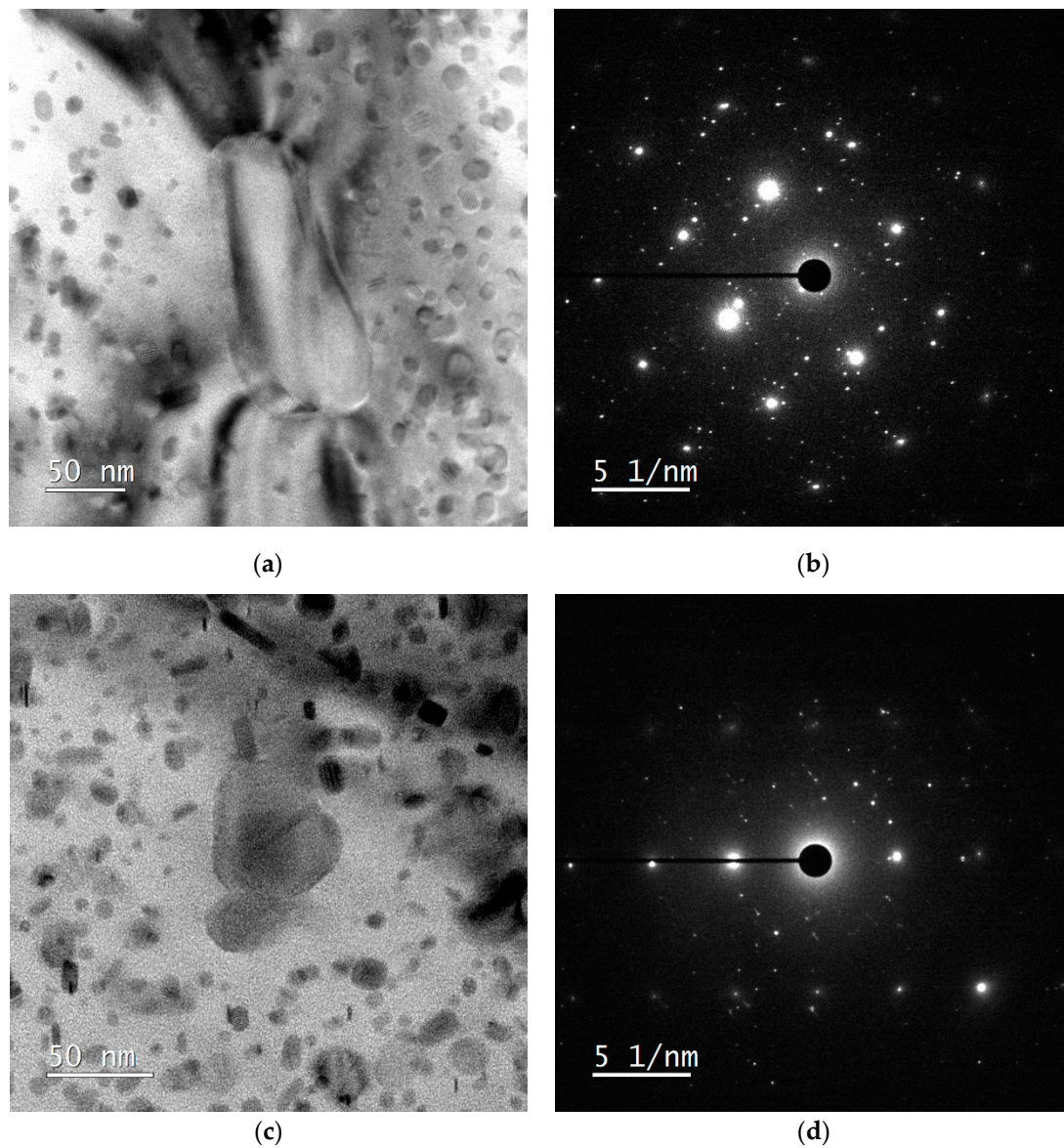


Figure 7. TEM photographs and diffraction patterns of Al_2CuMg precipitates in (a,b) the SO sample; (c,d) the HC sample.

Table 4. Potentiodynamic polarization measured for HC and SO samples (HC-A and SO-A: anodized samples); standard deviations are included in the parentheses.

| Sample Code | E_{corr} (V) | I_{corr} (A/cm^2) | E_{pit} (V) | I_{pit} (A/cm^2) |
|-------------|-----------------------|--|----------------------|---|
| HC | -1.30 (0.18) | $2.59 (1.49) \times 10^{-6}$ | -0.75 (0.03) | $4.35 (1.15) \times 10^{-5}$ |
| HC-A | -0.74 (0.04) | $7.97 (1.76) \times 10^{-7}$ | None visible | None visible |
| SO | -1.13 (0.06) | $4.40 (0.42) \times 10^{-6}$ | -0.79 (0.01) | $3.4 (1.13) \times 10^{-4}$ |
| SO-A | -0.91 (0.02) | $3.29 (1.07) \times 10^{-6}$ | None visible | None visible |

E_{corr} : corrosion potential; I_{corr} : corrosion current; E_{pit} : pitting potential; I_{pit} : pitting current.

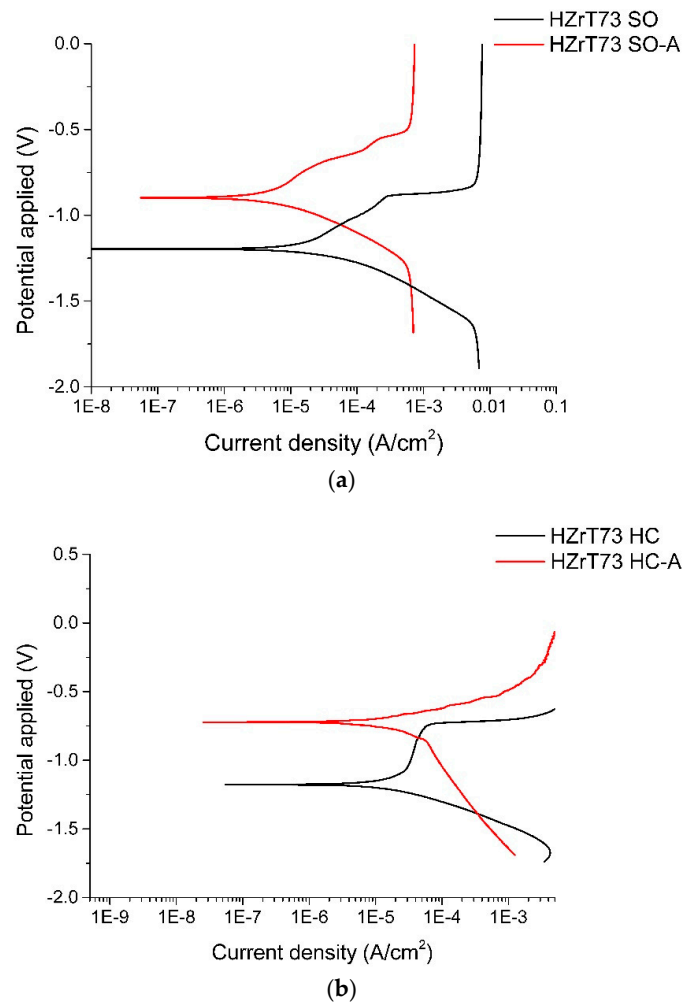


Figure 8. Polarization curves with or without anodization of (a) HZrT73 SO and (b) HZrT73 HC samples immersed in a 1 M NaCl solution.

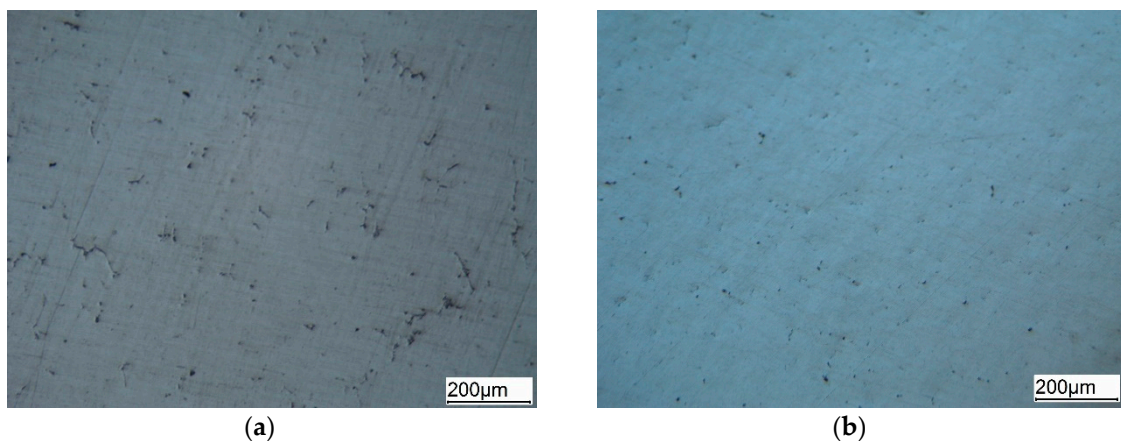


Figure 9. Optical micrographs showing a different content of intermetallic compound (IMC) (Al–Cu–Mg–Zn) particles in the matrix of (a) the HC sample and (b) the SO sample.

4. Conclusions

The Al–Zn–Mg–Cu alloys commonly deforms at a low strain rate in the industry. This study found that a cast/forged hybrid process with a high strain rate of $1\text{--}10^1\text{ s}^{-1}$ is effective to make Al alloys with high strength. After treating and deforming the cast blocks at a sub-zero temperature and

subjecting them to a T73 heat treatment, the forgings could reach the tensile strength of 484 MPa, YS of 407 MPa, and elongation of 11.8%. The Al alloys castings which are currently adopted in the industry mostly display a tensile strength of about 300 MPa and an elongation less than 10%. Our experimental results demonstrate the efficacy of an attractive cast/forge hybrid process to make Al alloy parts with a tensile strength over 400 MPa and an elongation over 10%.

The corrosion resistance of cast/forged Al-8Zn-2.5Mg-1.5Cu is exceptional, with E_{corr} of -1.13 – -1.3 V and I_{corr} of 2.59×10^{-6} – 4.4×10^{-6} A/cm². After anodization and sealing, the measured E_{corr} improved to -0.74 – -0.91 V and the I_{corr} enhanced to 3.29×10^{-6} – 7.97×10^{-7} A/cm². The material SO sample displayed corrosion resistance comparable to that of extruded AA7075 bar samples if anodization and sealed were employed.

Author Contributions: Investigation and data curation, E.-T.K.; writing—review and editing, T.-S.S.; software simulation, Y.-S.H.

Funding: This research was funded by the Ministry of Science and Technology in Taiwan, MOST 108-2221-E-008-047.

Acknowledgments: The authors greatly appreciate financial support and funding by the Ministry of Science and Technology in Taiwan (MOST 108-2221-E-008-047). Many thanks also to the National Central University for providing the SEM tests, to the National Chiao Tung University for the EBSD tests, and to the National Tsing Hua University for the TEM tests.

Conflicts of Interest: The authors declare no conflict of interest.

References

1. Abolhasani, A.; Zarei-Hanzaki, A.; Abedi, H.R.; Rokni, M.R. The room temperature mechanical properties of hot rolled 7075 aluminum alloy. *Mater. Des.* **2012**, *34*, 631–636. [[CrossRef](#)]
2. Ou, B.-L.; Yang, J.-G.; Yang, C.-K. Effects of step-quench and aging on mechanical properties and resistance to stress corrosion cracking of 7050 aluminum alloy. *Mater. Trans.* **2000**, *41*, 783–789. [[CrossRef](#)]
3. Wang, D.; Ma, Z.Y.; Gao, Z.M. Effects of severe cold rolling on tensile properties and stress corrosion cracking of 7050 aluminum alloy. *Mater. Chem. Phys.* **2009**, *117*, 228–233. [[CrossRef](#)]
4. Magalhães, D.C.C.; Hupalo, M.F.; Cintho, O.M. Natural aging behavior of AA7050 Al alloy after cryogenic rolling. *Mater. Sci. Eng. A* **2014**, *93*, 1–7.
5. Knight, S.P.; Pohl, K.; Holroyd, N.J.H.; Birbilis, N.P.; Rometsch, A.; Muddle, B.C.; Goswami, R.S.; Lynch, P. Some effects of alloy composition on stress corrosion cracking in Al-Zn-Mg-Cu alloys. *Corros. Sci.* **2015**, *98*, 50–62. [[CrossRef](#)]
6. Monda, L.C.; Mukhopadhyay, A.K. On the nature of T(Al₂Mg₃Zn₃) and S(Al₂CuMg) phases present in as-cast and annealed 7055 aluminum alloy. *Mater. Sci. Eng. A* **2005**, *391*, 367–376. [[CrossRef](#)]
7. Sha, G.; Cerezo, A. Early-stage precipitation in Al-Zn-Mg-Cu alloy (7050). *Acta Mater.* **2004**, *52*, 4503–4516. [[CrossRef](#)]
8. Li, J.-F.; Peng, Z.-W.; Li, C.-X.; Jia, Z.-Q.; Chen, W.-J.; Zheng, Z.-Q. Mechanical properties, corrosion behaviors and microstructures of 7075 aluminium alloy with various aging treatments. *Trans. Nonferrous. Met. Soc. China* **2008**, *18*, 755–762. [[CrossRef](#)]
9. Mahathaninwong, N.; Plookphol, T.; Wannasin, J.; Wisutmethangoon, S. T6 heat treatment of rheocasting 7075 Al alloy. *Mater. Sci. Eng. A* **2012**, *532*, 91–99. [[CrossRef](#)]
10. Ber, L.B. Accelerated artificial ageing regimes of commercial aluminium alloys. II: Al-Cu, Al-Zn-Mg-(Cu), Al-Mg-Si-(Cu) alloys. *Mater. Sci. Eng. A* **2000**, *280*, 91–96. [[CrossRef](#)]
11. Shih, T.-S.; Liao, T.-W.; Hsu, W.-N. Effects of Cryogenic Forging and Anodization on the Mechanical Properties of AA 7075-T73 Aluminum Alloys. *J. Mater. Eng. Perform.* **2016**, *25*, 1211–1218. [[CrossRef](#)]
12. Shih, T.-S.; Yong, H.-S.; Hsu, W.-N. Effects of cryogenic forging and anodization on the mechanical properties and corrosion resistance of AA6066-T6 Aluminum alloys. *Metals* **2016**, *6*, 51. [[CrossRef](#)]
13. Shih, T.-S.; Lin, J.-W. Mechanical properties and fatigue behavior of cast/forged Al-1.2%Mg-1.0%Si-1.0%Cu Aluminum alloys. *Mater. Trans.* **2018**, *59*, 1130–1134. [[CrossRef](#)]
14. Fujikawa, S.; Kitamura, Y.; Shimamura, S. Application of numerical methods for the aluminum casting/forging process. *J. Mater. Process. Technol.* **1991**, *27*, 93–110. [[CrossRef](#)]

15. Chang, F.C.; Hwang, W.S.; Lee, C.H.; Wu, C.F.; Yang, J.B. Forging condition for removing porosities in the hybrid casting and forging process of 7075 Aluminum alloy casting. *Mater. Trans.* **2004**, *45*, 1886–1890. [[CrossRef](#)]
16. Yang, Y.; Zhang, Z.; Li, X.; Wang, Q.; Zhang, Y. The effects of grain size on the hot deformation and processing map for 7075 aluminum alloy. *Mater. Des.* **2013**, *51*, 592–597. [[CrossRef](#)]
17. Deng, Y.-L.; Zhang, Y.-Y.; Li, W.; Zhu, A.A.; Zhang, X.-M. Three-stage homogenization of Al-Zn-Mg-Cu alloys containing trace Zr. *Metall. Mater. Trans. A* **2013**, *44*, 2470–2477. [[CrossRef](#)]
18. Shih, T.-S.; Chiu, Y.-W. Corrosion resistance and high-cycle fatigue strength of anodized/sealed AA7050 and AA7075 alloys. *Appl. Surf. Sci.* **2015**, *351*, 997–1003. [[CrossRef](#)]
19. Huang, Y.-S.; Shih, T.-S.; Chou, J.-H. Electrochemical behavior of anodized AA7075-T73 alloys as affected by the matrix structure. *Appl. Surf. Sci.* **2013**, *283*, 249–257. [[CrossRef](#)]
20. Muzyk, M.; Pakiel, Z.; Kurzydowski, K.J. Ab initio calculations of the generalized stacking fault energy in aluminum alloys. *Scr. Mater.* **2011**, *64*, 916–918. [[CrossRef](#)]
21. Jonas, J.J.; Quelennec, X.; Jiang, L.; Martin, É. The Avrami kinetics of dynamic recrystallization. *Acta Mater.* **2009**, *57*, 2748–2756. [[CrossRef](#)]
22. Feng, D.; Wang, G.; Chen, H.; Zhang, X.M. Effect of grain size inhomogeneity of ingot on dynamic softening behavior and processing map of Al-8Zn-2Mg-2Cu alloy. *Met. Mater. Int.* **2018**, *24*, 195–204. [[CrossRef](#)]
23. Feng, D.; Zhang, X.M.; Liu, S.D.; Deng, Y.L. Constitutive equation and hot deformation behavior of homogenized Al-7.68Zn-2.12Mg-1.98Cu-0.12Zr alloy during compression at elevated temperature. *Mater. Sci. Eng. A* **2014**, *608*, 63–72. [[CrossRef](#)]
24. Fan, X.-G.; Jiang, D.-M.; Meng, Q.-C.; Zhang, B.-Y.; Wang, T. Evolution of eutectic structures in Al-Zn-Mg-Cu alloys during heat treatment. *Trans. Nonferrous Met. Soc. China* **2006**, *16*, 577–581. [[CrossRef](#)]



© 2019 by the authors. Licensee MDPI, Basel, Switzerland. This article is an open access article distributed under the terms and conditions of the Creative Commons Attribution (CC BY) license (<http://creativecommons.org/licenses/by/4.0/>).